JACS
JOURNAL OF THE AMERICAN CHEMICAL SOCIETY

Communication

pubs.acs.org/JACS

Shape-Dependent Electrocatalytic Reduction of CO_2 to CO on Triangular Silver Nanoplates

Subiao Liu, Hongbiao Tao, Li Zeng, Qi Liu, Zhenghe Xu, Qingxia Liu,* and Jing-Li Luo*

Department of Chemical and Materials Engineering, University of Alberta, Edmonton, Alberta T6G 1H9, Canada

Supporting Information

ABSTRACT: Electrochemical reduction of CO_2 (CO_2RR) provides great potential for intermittent renewable energy storage. This study demonstrates a predominant shape-dependent electrocatalytic reduction of CO_2 to CO on triangular silver nanoplates (Tri-Ag-NPs) in 0.1 M $KHCO_3$. Compared with similarly sized Ag nanoparticles (SS-Ag-NPs) and bulk Ag, Tri-Ag-NPs exhibited an enhanced current density and significantly improved Faradaic efficiency (96.8%) and energy efficiency (61.7%), together with a considerable durability (7 days). Additionally, CO starts to be observed at an ultralow overpotential of 96 mV, further confirming the superiority of Tri-Ag-NPs as a catalyst for CO_2RR toward CO formation. Density functional theory calculations reveal that the significantly enhanced electrocatalytic activity and selectivity at lowered overpotential originate from the shape-controlled structure. This not only provides the optimum edge-to-corner ratio but also dominates at the facet of Ag(100) where it requires lower energy to initiate the rate-determining step. This study demonstrates a promising approach to tune electrocatalytic activity and selectivity of metal catalysts for CO_2RR by creating optimal facet and edge site through shape-control synthesis.

Increased utilization of fossil fuels has brought about record-breaking levels of atmospheric carbon dioxide (CO_2), which causes climate change and environmental issues.[1] To attenuate our reliance on fossil fuels, sustainable and environmentally friendly alternatives are desirable options. Electrochemical CO_2 reduction reaction (CO_2RR) points to a promising direction not only in decreasing CO_2 accumulation but also in converting intermittent renewable electricity into energy-dense fuels.[2] However, the more kinetically preferred H_2 evolution reaction (HER) always outcompetes the CO_2RR and consequently, decreases the selectivity of target product.[3] The high overpotential (η) is also required for CO_2RR to reach substantial reaction rates.[4] Therefore, it is desirable to search for novel catalysts capable of efficiently promoting CO_2RR with high selectivity (Faraday efficiency, FE) and catalytic activity (current density, j) at low η.

Various metallic electrocatalysts have been experimentally and computationally identified for CO_2RR because the binding energy of intermediate (CO*) on the metal surface is relatively weaker than that of H* derived from HER. This leads to the selective evolution of CO rather than the competitive H_2 on these metal surfaces. The existence of optimal particle size has also been reported to enhance strongly the catalytic activity for CO_2RR over metal-based catalysts, such as Au[5−7] and Ag,[8−13] where FE and current density reach maximum values. Zhu et al.[5] reported CO_2RR on Au nanoparticles (NPs) and found that the 8 nm Au NPs show FE up to 90% at −0.67 V (vs reversible hydrogen electrode, RHE). Ag NP, an attractive alternative for noble metal electrode, shows selectivity as high as that of Au at a lower cost. The size effects have also been observed by Cheonghee group[8] and they noted that 5 nm Ag/C has the best CO_2RR performance and achieves a maximum FE of 79.2% at −0.75 V vs RHE. It has been demonstrated that the enhanced size-dependent FE and current density are related to the ratio of edge-to-corner. Density functional theory (DFT) simulations also suggest that edge sites are more preferred for CO evolution than corner sites on sized-controlled noble metal NPs.[5,8,9,14] Recently, Min Liu et al.[15] also reported a field-induced reagent concentration that enables highly efficient CO_2RR resulting from local high electric fields. Besides the effects of size and local electric filed, understanding the shape effects of metal NP on CO_2RR is also worth noting. There have been limited studies on CO_2RR over metal NPs regarding the influence of particle shape, but further exploration is warranted because the presence of edge and corner sites varies as the shape changes.[5,9] Shape control has received extensive attention for Ag with particular emphasis on triangular Ag nanoplate (Tri-Ag-NP) because of their unique structure-related optical properties and potential applications.[16]

In this study, Tri-Ag-NPs were synthesized using a direct chemical reduction method.[17] The composite containing Tri-Ag-NPs and carbon black (CB) was fabricated on a glassy carbon electrode (GCE) for CO_2RR. It was found that Tri-Ag-NPs were particularly active for CO_2RR toward CO formation at an ultralow η. DFT calculations were employed to rationalize the increased catalytic activity and selectivity of Tri-Ag-NPs toward CO_2RR.

Tri-Ag-NPs were synthesized by chemically reducing an aqueous solution of $AgNO_3$ with $NaBH_4$ in the presence of H_2O_2 and trisodium citrate (Scheme 1).

UV/vis spectra were recorded to investigate the transformation process of Tri-Ag-NPs by judging from the spectra change, as shown in Figure 1a. Upon the rapid injection of $NaBH_4$, the color of the original transparent solution immediately became pale yellow, suggesting the occurrence of Ag reduction. Approximately 2 min after initiation, the pale solution turned deep yellow, an indication of Ag NP formation,

Received: November 23, 2016
Published: February 2, 2017

DOI: 10.1021/jacs.6b12103
J. Am. Chem. Soc. 2017, 139, 2160−2163

Scheme 1. Synthesis Process and Digital Images of Tri-Ag-NPs

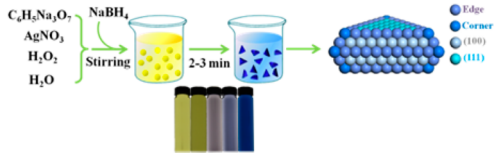

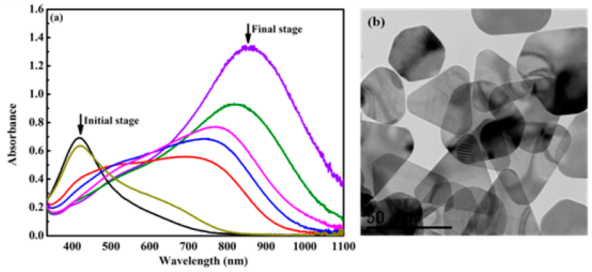

Figure 1. (a) UV/vis spectra; (b) TEM image of Tri-Ag-NPs.

as evidenced in the absorbance of the characteristic peak at ~400 nm,[17] where it quickly increased to the maximum. Subsequently, the solution quickly changed to blue, where the corresponding intensity of the characteristic peak of Ag NPs at ~400 nm quickly decreased, indicating the gradual consumption of Ag NPs during the transformation process. Another peak emerged at ~600 nm and gradually red-shifted to the wavelength of 850 nm, indicative of the formation and growth of Tri-Ag-NPs, as confirmed by the TEM image in Figure 1b. The Ag nanoplates obtained are enclosed by two (111) facets at both top and bottom surfaces, and three (100) facets at the side faces which contain twin planes and stacking faults along the vertical direction, as demonstrated by previous studies.[16,18]

To examine the CO_2RR activity of Tri-Ag-NPs, the mixture containing catalysts and CB was quantitatively dropped onto a GCE (0.785 cm^2). The polarization curves of all catalysts were obtained by a sweeping potential between −0.056 and −1.156 V vs RHE at a scan rate of 50 mV s^{-1}. Figure 2a shows the linear sweep voltammetry (LSV) results of Tri-Ag-NPs, SS-Ag-NPs and bulk Ag to distinguish the shape effects as well as CB and GCE as references to differentiate their contributions for CO_2RR. The Tri-Ag-NPs exhibited approximately 2-fold higher current densities (over 5.5 mA cm^{-2}, normalized by the geometrical surface area) relative to bulk Ag (3.0 mA cm^{-2}), and 1.0 mA cm^{-2} larger than SS-Ag-NPs. More importantly, a much more positive onset potential was observed for the Tri-Ag-NPs compared to the SS-Ag-NPs and to Bulk Ag. The increment in current density, indicative of a promoted cathodic kinetics for CO_2RR, is not conclusive evidence since HER and CO_2RR are often interconnected. To verify the occurrence of predominant CO_2RR other than HER, and the enhanced shape-dependent catalytic activity of Tri-Ag-NPs, potentiostatic electrolysis was carried out at different applied potentials. The achieved current densities are 30% less than the corresponding values in LSV measurements under the same potential load. This can be attributed to the combination of the presence of extra current from the interface charging, and the formation of a CO_2 and/or CO partially depleted layer in the vicinity of the catalyst due to the mass transport limitations.[19,20] The outlet gases were directly vented into a gas chromatography (GC) instrument to analyze quantitatively the gas composition. To confirm that the catalytic activity is not derived from bare GCE and CB, both samples were fabricated as the cathodes. GC analyses indicated that H_2 was the major product resulting from the competitive HER on GCE and CB (see Figure S7).

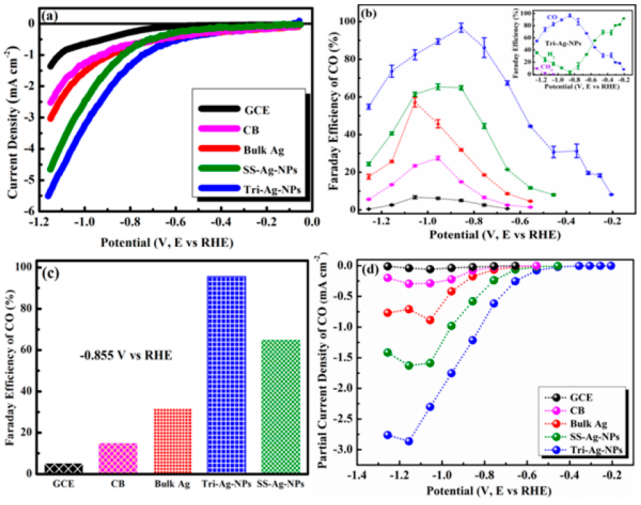

Figure 2. (a) Cathodic LSV results; (b) FEs of CO at various applied potentials (inset shows the CO, CH_4 and H_2 overall FE for Tri-Ag-NPs) and (c) CO FEs at fixed potential of −0.855 V; (d) CO partial current density.

Tri-Ag-NPs, SS-Ag-NPs and bulk Ag were also performed under the same experimental conditions, and the potential-dependent FEs for CO formation are shown in Figure 2b. CO (FE of 8.1%) started to generate at an onset potential of −0.206 V for Tri-Ag-NPs, which was only 96 mV lower than the theoretical equilibrium potential (−0.11 V) and remarkably lower than other reported Ag-based catalysts,[8,21] whereas CO was not detectable under this ultralow η (96 mV) for SS-Ag-NPs and bulk Ag. To achieve the equivalent FE for CO, SS-Ag-NPs (8.0%) and bulk Ag (8.6%) required a potential of −0.456 V (η of 346 mV) and −0.656 V (η of 546 mV), respectively. The FEs of CO increased significantly for Tri-Ag-NPs, SS-Ag-NPs and bulk Ag when more negative potentials were applied. Concurrently, Tri-Ag-NPs showed the best CO_2RR performance and reached its maximum value of 96.8% with a much lower η of 0.746 V as compared to SS-Ag-NPs (65.4%, 0.846 V) and bulk Ag (57.2%, 0.946 V). Comparing the FEs of all samples at a fixed potential of −0.856 V (Figure 2c), Tri-Ag-NPs showed 3- and 1.5-fold higher values than SS-Ag-NPs (64.9%) and bulk Ag (31.9%), respectively. This indicates that the CO_2RR is shape-dependent and the Tri-Ag-NPs are the most active for CO formation as compared to other reported Ag-based catalysts.[8,9,21] Figure 2d shows the potential-dependent CO partial current densities calculated based on the current densities from potentiostatic measurements and the corresponding CO FEs for all samples. It clearly reveals the exclusive catalytic activity of Tri-Ag-NPs for the CO_2RR toward CO formation, where a 2.2-fold increase in the CO partial current densities of Tri-Ag-NPs relative to SS-Ag-NPs further confirms the shape-dependent effects.

For comparing the reaction kinetics for CO_2RR and subsequently confirming the increased catalytic activity of Tri-Ag-NPs resulted from the shape control, Tafel plots for Tri-Ag-NPs, SS-Ag-NPs and bulk Ag are shown in Figure 3a.

The Tafel slope, an indication of kinetics for CO formation, was 153 mV dec^{-1} for Tri-Ag-NPs, closer to the value of 118

DOI: 10.1021/jacs.6b12103
J. Am. Chem. Soc. 2017, 139, 2160−2163

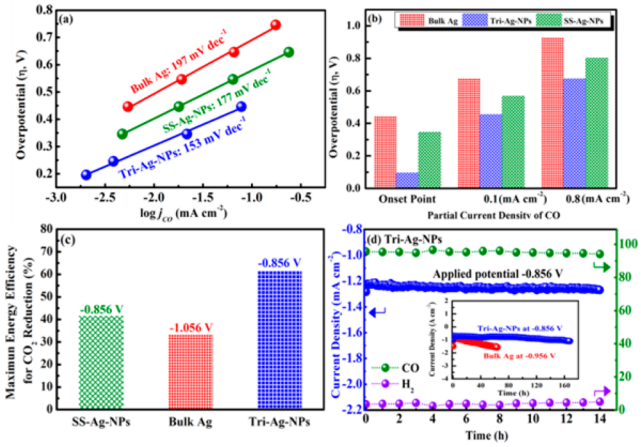

Figure 3. (a) Tafel plot and (b) η as a function of various current densities; (c) maximum energy efficiencies of Tri-Ag-NPs, SS-Ag-NPs and bulk Ag; (d) long-term stability at a potential load of −0.856 V and the corresponding FEs of CO and H_2.

mV dec^{-1} expected for rate-determining step at the electrode[22] as compared to a Tafel slope of 177 mV dec^{-1} for SS-Ag-NPs and 197 mV dec^{-1} for bulk Ag. Both values were larger than the one for Tri-Ag-NPs, indicating a poor kinetics for CO_2RR. Moreover, the formation of an adsorbed $*COO^-$ intermediate ($CO_2 + e^- \rightarrow *COO^-$) on catalyst surface exclusively determines the reaction rate for CO_2RR because the anionic radical is highly unstable. The negative reduction potential of the $CO_2/*COO^-$ redox couple, $E^o = -1.49$ vs RHE at pH 7, not only creates a significant thermodynamic and kinetic bottleneck for the overall CO_2RR but also promotes side reactions (e.g., HER) and consequently decreases the current efficiency for CO_2RR. However, the onset potential shifted anodically to −0.206 V on Tri-Ag-NPs (Figure 3b), a net decrease of 0.25 and 0.35 V in η compared to SS-Ag-NPs and bulk Ag, respectively. The exchange current density (i_o), a reflection of the free energy barrier required for CO_2RR at the reversible potential as well as a measure of intrinsic rate of electron transfer between the electrolyte and the electrode, was 1.1×10^{-4} mA cm^{-2} for Tri-Ag-NPs, 1 order of magnitude higher than that for SS-Ag-NPs (3.8×10^{-5} mA cm^{-2}) and bulk Ag (3.2×10^{-5} mA cm^{-2}). It is also comparable to a recently reported value (1.0×10^{-5} mA cm^{-2}) on 3 nm Ag/C for CO_2RR to CO,[8] further suggesting an improved shape-dependent catalytic activity. As a critical parameter in benchmarking electrocatalyst for renewable energy storage, the maximum energy conversion efficiencies of Tri-Ag-NPs, SS-Ag-NPs and bulk Ag were evaluated (Figure 3c). The low η together with the high FE of Tri-Ag-NPs contributed to an energy efficiency of over 61.7%, much higher than SS-Ag-NPs (42%) and bulk Ag (34%). This value is also comparable with the most efficient existing platforms for the formation of CO,[7,23] and consequently distinguishes Tri-Ag-NPs as a promising platform for CO_2RR.

To address the stability of the developed catalyst, a major concern for CO_2RR, the long-term performance of Tri-Ag-NPs was evaluated at a constant potential load of −0.856 V for 7 days. The outlet gases were analyzed each hour over a period of 14 h by GC. The corresponding FEs of CO and H_2 were also determined (Figure 3d), and the inset exhibits the long-term stability test over 7 days. The current density maintained a steady value at around −1.25 mA cm^{-2} with negligible degradation and the corresponding FEs of CO only fluctuated slightly around 96% throughout the stability test. Moreover, Tri-Ag-NPs show no morphological change after CO_2 reduction (Figure S9), further indicating the excellent stability of Tri-Ag-NPs for CO_2RR.

A better understanding on the origins credited for the ultralow onset potential, and the high CO selectivity at lower η for CO_2RR over shape-controlled Tri-Ag-NPs relative to SS-Ag-NPs, DFT calculations were further explored to investigate the reactivity of different Ag features based on the computational hydrogen electrode model.[5,9,14] Figure 4a shows the

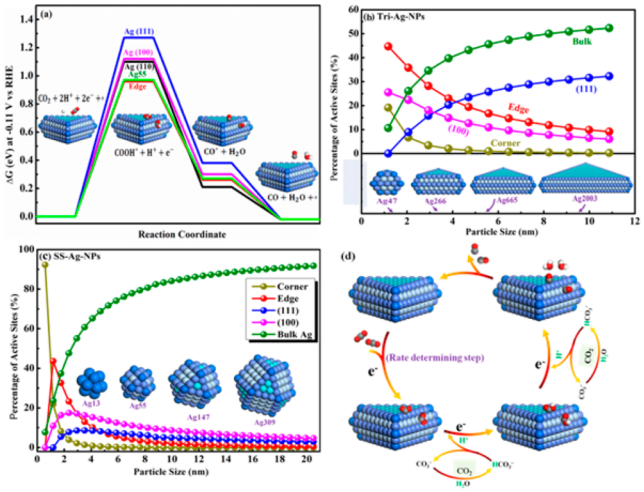

Figure 4. (a) Free energy diagrams for CO_2RR to CO on different facets and Ag55 cluster at −0.11 V; active adsorption site density on (b) Tri-Ag-NPs and (c) SS-Ag-NPs as a function of particle size; (d) proposed mechanism for CO_2RR to CO on Tri-Ag-NPs.

Gibbs free energy (ΔG) diagram for CO_2RR on different facets and Ag55 cluster, where the total ΔG values required for the proposed four elementary reaction steps were simulated and calculated (Figure 4d). The required η initially originates from the formation of COOH* because an uphill energy barrier of the first proton-coupled electron-transfer step for all facets and the cluster was observed. Apparently, the required ΔG to form the COOH* on Ag(100) is significantly lower than that on Ag(111) and quite close to the one on Ag(110), suggesting a higher catalytic activity of Ag(100) for CO_2RR. More importantly, the facet of (100) is predominant in Tri-Ag-NPs as compared to that in SS-Ag-NPs because Tri-Ag-NPs are only enclosed by the facets of (100) and (111). The free-energy step subsequently becomes more thermodynamically facile for the second proton-coupled electron transfer for the adsorbed CO* at all facets. Although the Ag55 cluster is slightly easier for the formation of COOH* than all facets, it tends to overbind with CO* and consequently decreases the product evolution rate. Thus, both the dominance of (100) and the ease in the CO evolution deriving from the shape-controlled effect point to the decreased η and low onset potential for CO formation. Additionally, studies have demonstrated that an increased edge-to-corner ratio yields enhanced catalytic activity and selectivity for CO_2RR because the adsorption of CO_2 and the subsequent formation of intermediate COOH* are easier on edge sites than corner sites.[5,9,14] Thus, the edge-to-corner ratios of Tri-Ag-NPs and SS-Ag-NPs as a function of the cluster diameter were also analyzed (Figure 4b,c). It is found that Tri-Ag-NPs with a diameter range from 0 to 12 nm maintain a comparably

DOI: 10.1021/jacs.6b12103
J. Am. Chem. Soc. 2017, 139, 2160−2163

higher edge-to-corner ratio. Although the ratio difference between Tri-Ag-NPs and SS-Ag-NPs narrows gradually at larger diameters, the density of catalytically active edge sites on Tri-Ag-NPs always exceeds that on SS-Ag-NPs. This ensures sufficient active edge sites for CO_2 reduction to CO and consequently leads to superior selectivity of Tri-Ag-NPs.

In summary, we successfully synthesized Tri-Ag-NPs and investigated its shape-dependent electrocatalytic reduction of CO_2 to CO in 0.1 M $KHCO_3$. Tri-Ag-NPs exhibit considerably higher selectivity as compared to SS-Ag-NPs and bulk Ag. Moreover, CO can be detected at an ultralow onset potential, confirming the excellent catalytic activity of Tri-Ag-NPs toward CO_2RR. The durability test over 7 days further confirms the excellent performance of Tri-Ag-NPs for efficient CO_2RR. DFT calculations indicate that the high selectivity of Tri-Ag-NPs at an ultralow overpotential is a consequence of both the optimum edge-to-corner ratio and the predominant Ag(100) facet in Tri-Ag-NPs.

■ ASSOCIATED CONTENT

Supporting Information

The Supporting Information is available free of charge on the ACS Publications website at DOI: 10.1021/jacs.6b12103.

Experimental details (PDF)

■ AUTHOR INFORMATION

Corresponding Authors

*qingxia2@ualberta.ca
*luoj@ualberta.ca

ORCID

Subiao Liu: 0000-0001-6075-3301
Zhenghe Xu: 0000-0001-8118-1920

Notes

The authors declare no competing financial interest.

■ ACKNOWLEDGMENTS

This work was supported by the Natural Sciences and Engineering Research Council of Canada.

■ REFERENCES

(1) Buitenwerf, R.; Rose, L.; Higgins, S. I. *Nat. Clim. Change* **2015**, *5*, 364−368.
(2) Goeppert, A.; Czaun, M.; May, R. B.; Prakash, G. S.; Olah, G. A.; Narayanan, S. *J. Am. Chem. Soc.* **2011**, *133*, 20164−20167.
(3) Qiao, J.; Liu, Y.; Hong, F.; Zhang, J. *Chem. Soc. Rev.* **2014**, *43*, 631−675.
(4) Costentin, C.; Robert, M.; Savéant, J.-M. *Chem. Soc. Rev.* **2013**, *42*, 2423−2436.
(5) Zhu, W.; Michalsky, R.; Metin, O.; Lv, H.; Guo, S.; Wright, C. J.; Sun, X.; Peterson, A. A.; Sun, S. *J. Am. Chem. Soc.* **2013**, *135*, 16833−16836.
(6) Koh, J. H.; Jeon, H. S.; Jee, M. S.; Nursanto, E. B.; Lee, H.; Hwang, Y. J.; Min, B. K. *J. Phys. Chem. C* **2015**, *119*, 883−889.
(7) Chen, Y.; Li, C. W.; Kanan, M. W. *J. Am. Chem. Soc.* **2012**, *134*, 19969−19972.
(8) Kim, C.; Jeon, H. S.; Eom, T.; Jee, M. S.; Kim, H.; Friend, C. M.; Min, B. K.; Hwang, Y. J. *J. Am. Chem. Soc.* **2015**, *137*, 13844−13850.
(9) Back, S.; Yeom, M. S.; Jung, Y. *ACS Catal.* **2015**, *5*, 5089−5096.
(10) Hatsukade, T.; Kuhl, K. P.; Cave, E. R.; Abram, D. N.; Jaramillo, T. F. *Phys. Chem. Chem. Phys.* **2014**, *16*, 13814−13819.
(11) Salehi-Khojin, A.; Jhong, H.-R.; Rosen, M. B. A.; Zhu, W.; Ma, S.; Kenis, P. J. A.; Masel, R. I. *J. Phys. Chem. C* **2013**, *117*, 1627−1632.
(12) Yoon, Y.; Hall, A. S.; Surendranath, Y. *Angew. Chem.* **2016**, *128*, 15508−15512.
(13) Lu, Q.; Rosen, J.; Zhou, Y.; Hutchings, G. S.; Kimmel, Y. C.; Chen, J. G.; Jiao, F. *Nat. Commun.* **2014**, *5*, No. 3242.
(14) Gao, D.; Zhou, H.; Wang, J.; Miao, S.; Yang, F.; Wang, G.; Wang, J.; Bao, X. *J. Am. Chem. Soc.* **2015**, *137*, 4288−4291.
(15) Liu, M.; Pang, Y.; Zhang, B.; De Luna, P.; Voznyy, O.; Xu, J.; Zheng, X.; Dinh, C. T.; Fan, F.; Cao, C.; de Arquer, F. P.; et al. *Nature* **2016**, *537*, 382−386.
(16) Xia, Y.; Xiong, Y.; Lim, B.; Skrabalak, S. E. *Angew. Chem., Int. Ed.* **2009**, *48*, 60−103.
(17) Zhang, Q.; Li, N.; Goebl, J.; Lu, Z.; Yin, Y. *J. Am. Chem. Soc.* **2011**, *133*, 18931−18939.
(18) Zeng, J.; Xia, X.; Rycenga, M.; Henneghan, P.; Li, Q.; Xia, Y. *Angew. Chem., Int. Ed.* **2011**, *50*, 244−249.
(19) Kumar, B.; Asadi, M.; Pisasale, D.; Sinha-Ray, S.; Rosen, B. A.; Haasch, R.; Abiade, J.; Yarin, A. L.; Salehi-Khojin, A. *Nat. Commun.* **2013**, *4*, No. 2819.
(20) Asadi, M.; Kim, K.; Liu, C.; Addepalli, A. V.; Abbasi, P.; Yasaei, P.; Phillips, P.; Behranginia, A.; Cerrato, J. M.; Haasch, R.; et al. *Science* **2016**, *353*, 467−470.
(21) Hsieh, Y. C.; Senanayake, S. D.; Zhang, Y.; Xu, W.; Polyansky, D. E. *ACS Catal.* **2015**, *5*, 5349−5356.
(22) Zhang, S.; Kang, P.; Ubnoske, S.; Brennaman, M. K.; Song, N.; House, R. L.; Glass, J. T.; Meyer, T. J. *J. Am. Chem. Soc.* **2014**, *136*, 7845−7848.
(23) Rosen, B. A.; Salehi-Khojin, A.; Thorson, M. R.; Zhu, W.; Whipple, D. T.; Kenis, P. J.; Masel, R. I. *Science* **2011**, *334*, 643−644.

DOI: 10.1021/jacs.6b12103
J. Am. Chem. Soc. 2017, 139, 2160−2163